EUMETSAT AC SAF
ATMOSPHERIC COMPOSITION MONITORING

ALGORITHM THEORETICAL BASIS DOCUMENT

IASI NRT SO2 column and altitude L2 (O3M-379)

IASI Reprocessed SO2 column and altitude L2 CDR (O3M-540) Metop-A&B

Prepared by	Lieven Clarisse Daniel Hurtmans Pierre-François Coheur Rosa Astoreca Camille Viatte Juliette Hadji-Lazaro	March 9, 2023

DOCUMENT STATUS SHEET

Issue	Date	Modified items / Reason for change
1.0	16/11/2015	First version of the Brescia ATBD.
1.1	28/07/2016	Graphic representation of the retrieval sequence of the Brescia SO_2 algorithm was added.
1.2	24/09/2020	SO2 altitude retrieval algorithm added to the ATBD
1.3	01/02/2021	MTR Reviewer's comments added to the ATBD.
1.4	09/03/2023	Added product identifier in cover page for NRT SO2 column and altitude and SO2 CDR. Added description of the SO2 CDR in section 1.1 for the MTR.

TABLE OF CONTENTS

1. INTRODUCTION

1.1 Objective

This document describes the Brescia SO_2 columns and SO_2 altitude retrieval algorithms for IASI developed at the Université Libre de Bruxelles (ULB; Clarisse et al., 2012, 2014) which have been partially implemented at EUMETSAT in the frame of the AC SAF CDOP-2 and CDOP-3 projects.

The IASI SO2 L2 CDR has been reprocessed at EUMETSAT using IASI NRT SO2 produced with Brescia v20180401_sp20200222.

Please note that this ATBD mainly refers to the IASI NRT SO2, from which the IASI SO2 CDR is generated, and that has been extensively reviewed during CDOP-2 and CDOP-3.

1.2 IASI instrument

IASI is an infrared Fourier transform spectrometer developed jointly by CNES (the French space agency) with support of the scientific community (for a review see Hilton et al. (2011)), and by EUMETSAT. IASI is mounted on-board the European polar-orbiting Metop satellite with the primary objective to improve numerical weather predictions, by measuring tropospheric temperature and humidity with high horizontal resolution and sampling, with 1 km vertical resolution, and with respectively 1 K and 10% accuracy (Camy-Peyret and Eyre, 1998). As a second priority IASI contributes to atmospheric composition measurements for climate and chemistry applications (Clerbaux et al., 2009). To reach these two objectives, IASI measures the infrared radiation of the Earth's surface and of the atmosphere between 645 and 2760 cm^{-1} at nadir and along a 2200 km swath perpendicular to the satellite track. A total of 120 views are collected over the swath, divided as 30 arrays of 4 individual Field-of-views (FOVs) varying in size from 36 $\times\pi$ km^2 at nadir (circular 12 km diameter pixel) to 10 x 20 x π km^2 at the larger viewing angle (ellipse-shaped FOV at the end of the swath). IASI offers in this standard observing mode global coverage twice daily, with overpass times at around 9:30 and 21:30 mean local solar time. The very good spatial and temporal sampling of IASI is complemented by fairly high spectral and radiometric performances: the calibrated level 1C radiances are at 0.5 cm^{-1} apodized spectral resolution (the instrument achieves a 2 cm optical path difference), with an apodized noise that ranges below 2500 cm^{-1} between 0.1 and 0.2 K of a reference blackbody at 280 K (Hilton et al., 2011).

1.3 Product characteristics overview and context

In this document, two algorithms are described. The first algorithm for the sounding of SO_2 above ~5 km altitude using high resolution infrared sounders, such as IASI, is outlined in section 2. The main features of this algorithm are a wide applicable total column range (over 4 orders of magnitude, from 0.5 to 5000 dobson units), a low theoretical uncertainty (3-5 %) and near real time applicability. The output consists of 5 different hypothetical SO_2 columns, depending on the altitude of the SO_2 plume in question, and is meant to be used with auxiliary altitude data. A typical use-case is where a user will have an estimate of the SO_2 altitude (provided by e.g. a model

or third party measurements), and in that case, can interpolate the 5 SO_2 columns to this estimate to obtain a single SO_2 column.

Information on the SO_2 altitude can also be retrieved directly from the IASI measurements, and this is what the second algorithm aims at. This product has its applications in its own right. In addition, an interpolated SO_2 column (from the first algorithm), at the retrieved SO_2 altitude (from the second algorithm) is also provided. In case the user has no information on the SO_2 altitude and is interested in the SO_2 column, it is recommended that this interpolated SO_2 column product is used.

The data flow of the two algorithms and how they are linked is illustrated in Figure 1.

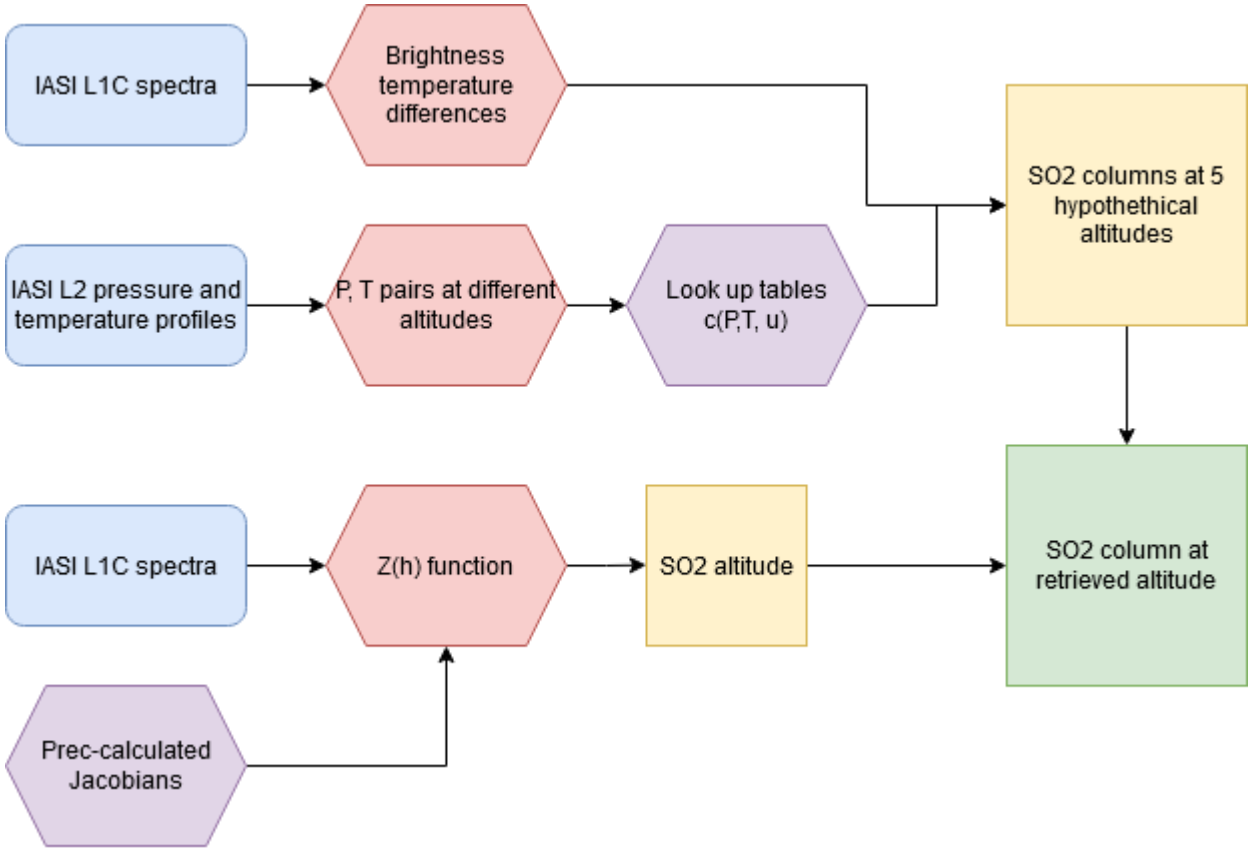

Figure 1: Graphic representation of the retrieval sequence of the Brescia SO_2 column and altitude algorithm.

There are currently several atmospheric sounders able to provide total column of SO_2, both in the UV and TIR, e.g. IASI, AIRS, OMI, GOME-2, OMPS. What differentiates SO_2 soundings with IASI from other sounders is its high sensitivity and robustness to mid-troposphere lower-stratosphere UTLS SO_2, and the combination of twice daily global coverage and a relative small footprint, 12km at nadir for IASI as compared to 13.5km at nadir for AIRS, 13x24 km² for OMI, 40/80 x 40 km² for GOME and 50x50 km² for OMPS. The SO_2 altitude algorithm is unique in its type.

2. THE IASI BRESCIA SO_2 COLUMN ALGORITHM

2.1 Algorithm description

Note that most of the algorithm description below is reproduced verbatim from Clarisse et al. (2012).

Sulphur dioxide has three absorption bands in the mid infrared, see Fig. 2. The ν_3 is by far the strongest band. Competing water vapor absorption limits its vertical sensitivity to SO_2 above 3-5 km, depending on the humidity profile and SO_2 abundance. Higher altitude SO_2 is also affected, directly, by water vapor in and above the SO_2 layer, but also indirectly by variable radiation coming from below. The ν_1 band is situated in an atmospheric window, and can penetrate the lower troposphere. While water vapor is not as important here, the 800-1200 cm^{-1} region is very sensitive to the surface temperature, surface emissivity and volcanic ash (Clarisse et al., 2010 a,b), and for young volcanic plumes from explosive eruptions, SO_2 and ash often need to be retrieved simultaneously. The combination band $\nu_1+\nu_3$ can only be used when there is reflected solar light. It is weak, but has been applied for the study of major volcanic eruptions as an alternative to a saturating ν_3 band (Karagulian et al., 2010; Prata et al., 2010). Note that all TIR measurements require thermal contrast defined here as the contrast difference between the SO_2 plume and the underlying radiation. Typically a value of 5K should be enough for an accurate retrieval. While the occurrence of favourable conditions is hard to quantify, in general thermal contrast will be lower for lower assumed altitudes, the occurrence of clouds and in humid conditions (e.g. the tropical latitude band). No land/ocean dependence is expected as the spectral channels which are used are not in an atmospheric window, and thus not sensitive to the surface.

In what follows, we assume an atmosphere with a SO_2 cloud present at a given altitude. We adopt the notations from Watson et al. (2004). When the plume is at sufficient altitude (where the absorption of other species can be ignored) the measured radiance L_s at a wavenumber ν (and corresponding measured brightness temperature at the sensor T_s) can be approximated as

$$L_s(\nu) = L_{ucb}(\nu)t_c + L_c(\nu)(1-t_c), \quad (1)$$

with $L_c(\nu) = B(\nu, T_c)$ the ambient radiance coming from the cloud at temperature T_c and specified by Planck's law, $L_{ucb}(\nu)$ the upwelling radiance at the cloud base and t_c the transmission of the cloud, given by the Bouguer-Lambert-Beer law

$$t_c = e^{-cu}, \quad (2)$$

with c an absorption coefficient dependent on pressure and temperature and u the column abundance. While Eq.(1) is valid under the mentioned assumptions, a subtlety arises when applying it to real measurements. Real radiance measurements are always integrated (convolved) over a wavenumber interval and are altered by the instrumental line shape. To check to what extent Eq.(1) holds at the level of finite microwindows (here IASI channels), we have simulated the radiative transfer of a standard atmosphere and introduced a SO_2 layer at a fixed altitude, but with varying abundances. The RTM is Atmosphit (Coheur et al, 2005). Atmosphere is taken from US Standard Atmosphere (NASA, 1976) and linelist from HITRAN (Rothman et al., 2003).

The results are shown in Fig. 3 in brightness temperature space at wavenumber $\nu = 1371.75\ \mathrm{cm}^{-1}$. The simulations are shown as black squares and the best fit with Eq. (1) (best choice of the absorption coefficient c) is shown in red. For a plume at high pressure (left panel, 450 hPa), an almost perfect fit can be obtained. The asymptotic behavior for increasingly large abundances can also be observed $(L_s(\nu) \rightarrow B(\nu, T_c)$ or $T_s \rightarrow T_c)$. This saturation is slower for lower pressure (right panel, 10 hPa). At very low pressure, spectral lines saturate at a lower concentration at their line centers than their wings. In contrast, at a higher pressure, pressure broadening of the individual lines is important and will distribute absorption over a wider spectral range, resulting in a net larger absorption and thus a quicker saturation over the complete band when taking into account all spectral lines. For the low pressure test case, a good fit with Eq.(1) and a constant absorption coefficient c is not possible. Because of the lower pressure broadening, the instrumental line shape and apodisation become relatively more important, and these effects are not taken into account in Eq.(1). One way to resolve this is to introduce an explicit column dependence in the coefficient c, so that $c = c(T, P, u)$. These coefficients can be estimated from forward simulations as outlined in the next section.

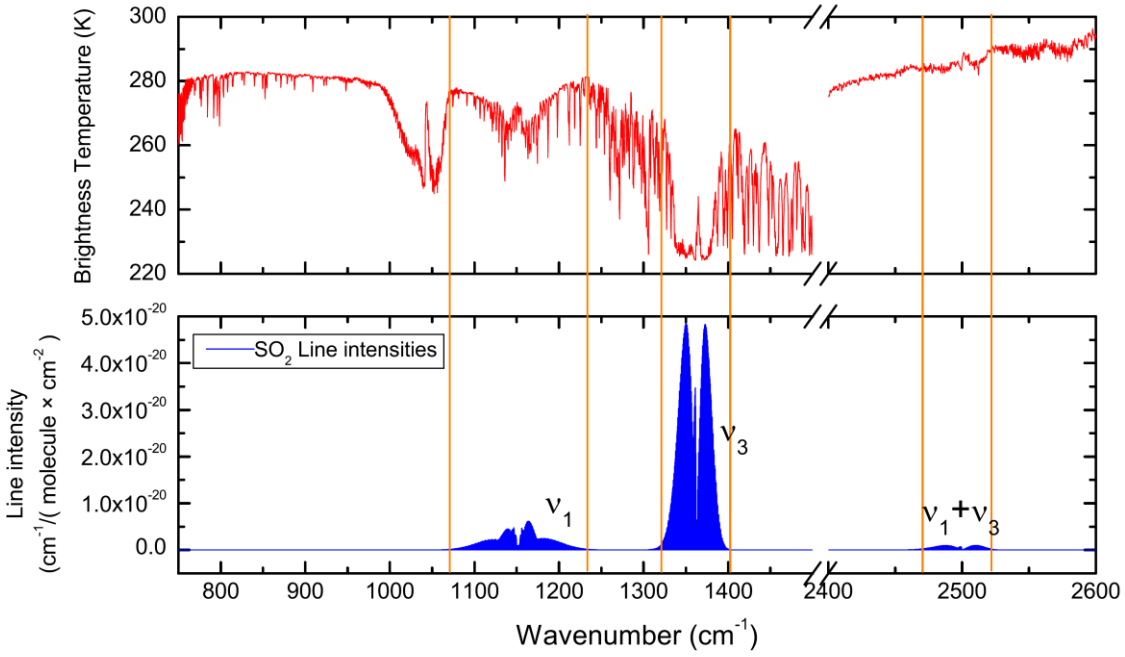

Fig. 2. Top panel: example IASI spectrum measured over the plume of the August 2008 eruption of Kasatochi. Bottom panel: line positions and intensities of SO_2 from HITRAN (see Rothman et al., 2009, and references therein). Band centers and integrated band intensities of SO_2 are (see Flaud et al., 2009, and references therein): the ν_1 symmetric stretch (~1152 cm^{-1} = 8.7 μm at 0.35×10−17 cm^{-1}/(molecule cm^{-2})), the ν_3 asymmetric stretch (~1362 cm^{-1} = 7.3 μm at 2.72×10−17 cm^{-1}/(molecule cm^{-2})) and the $\nu_1+\nu_3$ combination band (~2500 cm^{-1} = 4 μm at 0.054×10^{-17} cm^{-1}/(molecule cm^{-2})).

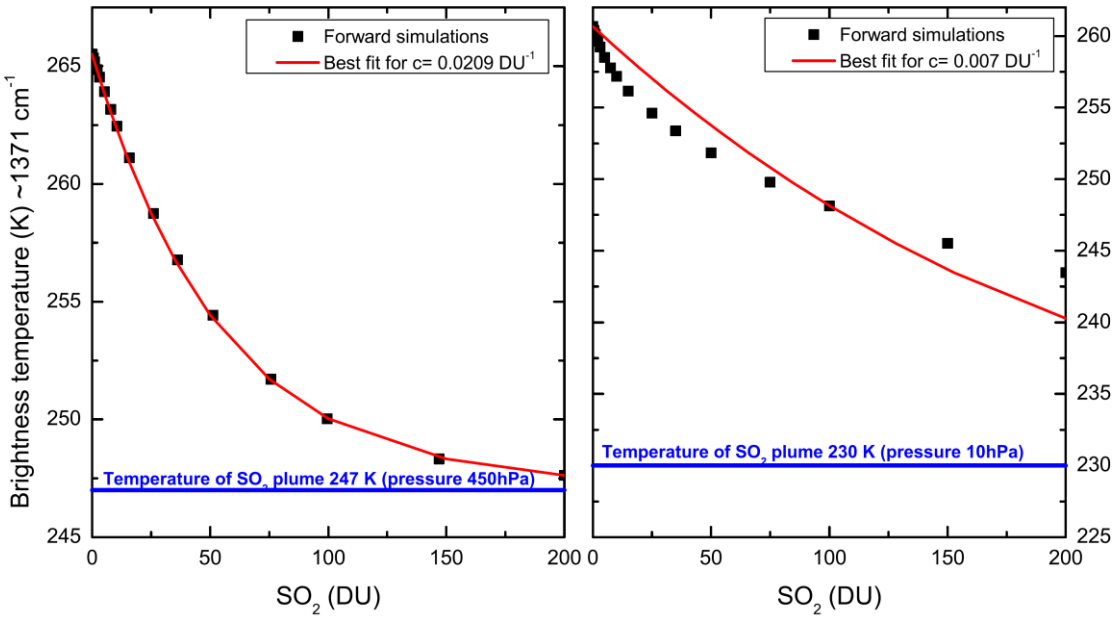

Fig. 3. Brightness temperature at 1371.75 cm^{-1} as a function of SO_2 mass loading for a low (left, plume at 247K and 450 hPa ~5 km) and high (right, plume at 230K and 10 hPa ~25 km) altitude plume. The colored black squares were calculated from simulated IASI spectra, while the red full line is a best fit of these simulations with Eq. (1).

To determine the SO_2 abundance from Eq. (1), all that is left is to estimate $L_{ucb}(\nu)$. This can be done from channels not affected by SO_2, but for which the channel ν responds similarly to H_2O and other atmospheric parameters than the channels sensitive to SO_2. It is here easier to work in brightness temperature space, where Eq. (1) reads

$$B(T_s,\nu) = B(T_{ucb},\nu)t_c + B(T_c,\nu)(1-t_c). \quad (3)$$

Now T_{ucb} can be estimated from another channel ν' when for background concentrations of SO_2

$$T_s = B^{-1}(L_s(\nu),\nu) \approx B^{-1}(L_s(\nu'),\nu') = T_{ucb}. \quad (4)$$

The critical part is to choose these channels ν and ν' to make this estimate as good as possible. Two sets of two pairs of background and SO_2 channels have been used: two to estimate T_s, representing the absorption in the ν_3 band and two reference channels to estimate T_{ucb}. Table 1 lists two sets of such parameters together with their bias and standard deviation (estimated from a full day of IASI measurements with no detectable volcanic SO_2). Note that this doubling of channels allows to reduce the standard deviation significantly and also that the bias can be subtracted in the calculation of the brightness temperature difference. Figure 4 illustrates the sensitivity range of both sets for a plume at 150 hPa. The absorption channels in the ν_3 band of the first set are chosen close to the region of maximum absorption, around 1371.75 cm^{-1}. It is sensitive to mass loadings as low as 0.5 DU, but saturates at around 200 DU, above which differences in the observed channels become too small. The second set has its absorption channels further away from the band center, at 1385 cm^{-1}. It has a lower sensitivity of about 10 DU, but can measure columns up to 5000 DU. The combined use of both sets therefore enables to retrieve columns of SO_2 from about 0.5 to 5000 DU at 150 hPa.

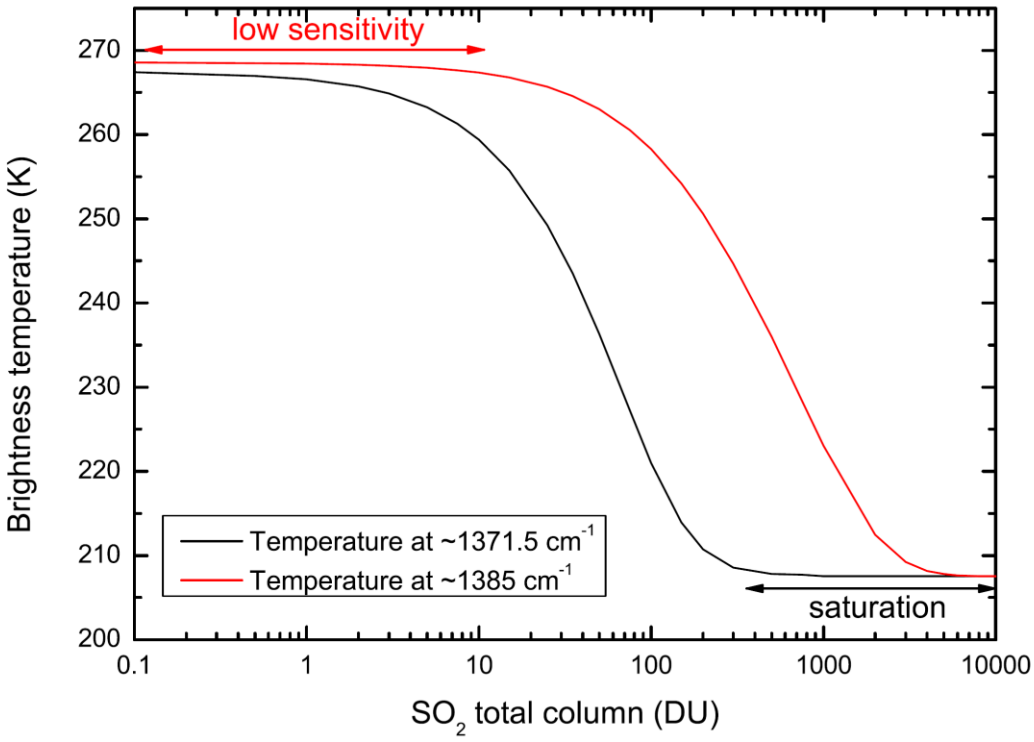

Fig. 4. Brightness temperature of the two sets of absorption channels (at ~1371.5 cm^{-1} and at ~1385 cm^{-1}) as a function of SO_2 abundance for a plume located at 150 hPa and 207 K. Note that these are simulated results. The RTM used was Atmosphit (Coheur et al., 2005).

Table 1: Two sets of absorption and background channels used in the calculation of SO_2 abundances. The mean and standard deviation of their brightness temperature differences between real measurements made in SO_2-free observations (1 full day) in the selected background and SO_2 channels.

	ν_3 Absorption channels	Background channels	Mean	Std
Set 1	1371.50, 1371.75 cm^{-1}	1407.25, 1408.75 cm^{-1}	-0.05 K	0.15 K
Set 2	1384.75, 1385.00 cm^{-1}	1407.50, 1408.00 cm^{-1}	0.05 K	0.25 K

Equation (1) is only valid when no absorption above the SO_2 plume takes place. Even at altitudes above ~500 hPa altitude, some residual water absorption can still affect observed channels. Assuming that water vapour above is colder than the SO_2 plume (so disregarding significant water vapor above lower stratospheric plumes), we have for a saturating cloud $T_s < T_c$. We therefore introduce a virtual cloud temperature $T_c^* = T_c - [H_2O]/10^{21}$, with [$H_2O$] the partial column of water (in molecules cm^{-2}) above the SO_2 layer . The factor 10^{21} was determined empirically, and while this is a first order correction, it is largely sufficient as we will see below.

2.2 Generation of the $c(T,P,u)$ look up table

To calculate the absorption coefficients $c(T,P,u)$ we have used representative atmospheric profiles (temperature, pressure, humidity and ozone) from the ECMWF 40-yr reanalysis, ERA-40 (Chevallier, 2001). The total set contains 13495 well sampled profiles. Pressure and temperature (PT) pairs between 5 and 30 km altitude are plotted in Fig. 5. The visible pressure bands are an artifact caused by the specific 60-level coordinate system in the data set, and these disappear when working with the interpolated data. We have calculated $c(T,P,u)$ on a subgrid of this PT diagram, indicated by the black dots.

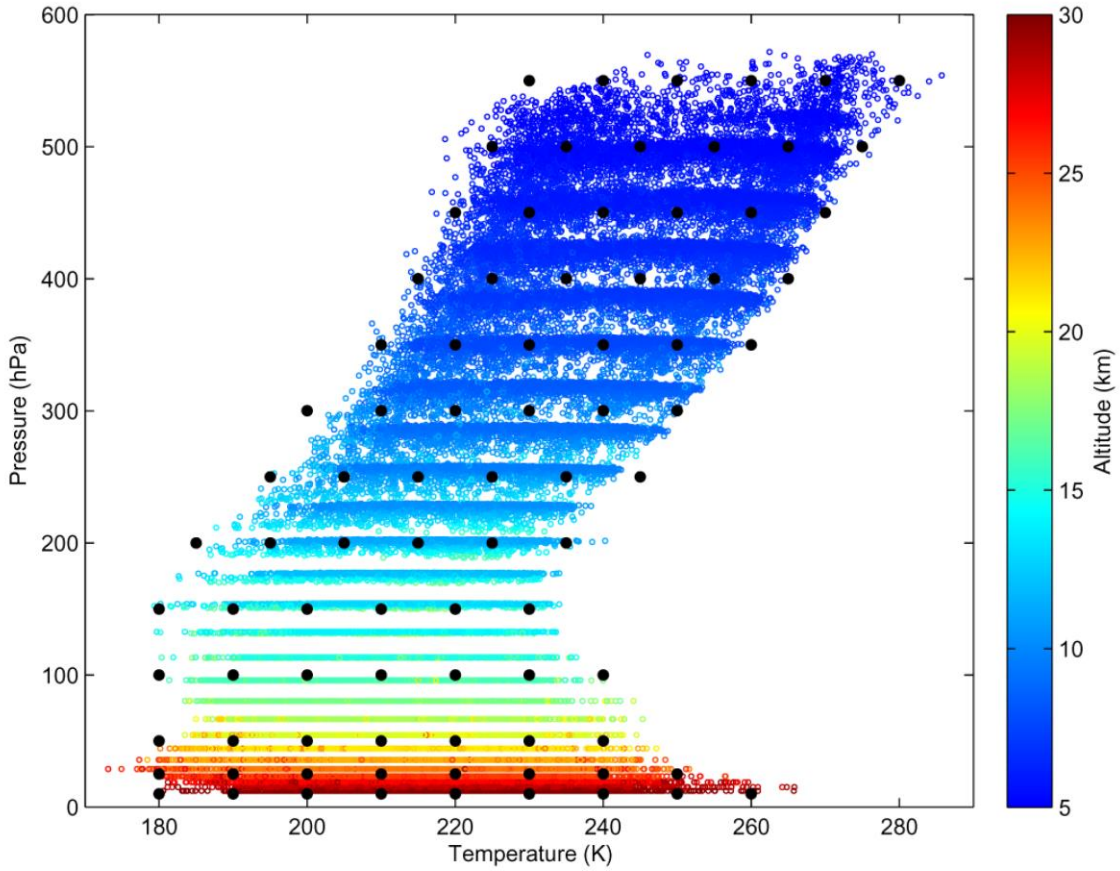

Fig. 5. Pressure and temperature correlations of the ERA-40 data set between 5 and 30 km. The black dots are the PT pairs for which the lookup tables were built.

For each PT pair in the subgrid, we selected 10 atmospheres from ERA-40 with the closest match in the PT profile. A variable SO_2 cloud (from 0 to 10000 DU) was then inserted at the altitude corresponding to the PT pair and the resulting IASI spectrum was simulated. Based on these simulations a best value for $c(T,P,u)$ was obtained from minimizing the relative error between the real and the calculated SO_2 abundance. Each $c(T,P,u)$ is obtained from 10 independent simulations and determining the best value is therefore an over-constrained problem. The solution however is guaranteed not to be overly dependent on an individual atmosphere, and the average relative error is

a good indication for the theoretical error (caused by the variability of other atmospheric parameters) which can be achieved with this algorithm.

The top panel in Fig. 6 shows the absorption coefficients for the two sets of channels at 10 and 750 DU respectively. For 4 PT pairs, T_{ucb} was very close or inferior to T_c for all 10 profiles. These sets of low thermal contrast or temperature inversion were excluded. These are situated at the very edge of the PT space and are uncommon. The bottom panel shows the mean relative error between the input SO_2 abundance and the retrieved for the ten different profiles. Errors are less than 3 % and 5 % for the first and second set respectively, except again at some points at the edge of the PT space.

We end this section with a practical consideration, which is important in the implementation of the above retrieval algorithm. The use of $c(T,P,u)$ to calculate the column abundance u is inherently a recursive problem. The iterative mechanism works by first applying a first guess value for c, which allows a calculation of the column. This then allows using a more appropriate c(T,P,u). This process is repeated 10 times (in practice convergence is achieved very quickly, after 2-3 times).

It is therefore necessary to start with a first guess $c(T,P)$ and iteratively calculate u and $c(T,P,u)$ until convergence is achieved. We have verified numerically that this convergence is always achieved (due to the smooth and monotonous behavior of the c coefficients). Also note that we find two estimates u_1 and u_2 for u, for each set of absorption and background channels. Theoretically, these two estimates should only agree when the assumed altitude corresponds to the real altitude (because the corresponding brightness temperature differences have a different pressure and temperature dependence). From looking at a few test cases, the two estimates generally agree well between 25 DU and 75 DU (with a standard deviation of around 10 %). On either side of this range, differences increase, with the u_1 estimate obviously superior for lower total column amounts and the u_2 estimate by construction superior for large column total amounts. When either u_1 or u_2 exceed 100 DU, we used the u_2 estimate, otherwise u_1 was used. Finally, the retrieval is also preceded by a detection criterion, here taken to be $T_{ucb} - T_s > 0.4\text{K}$.

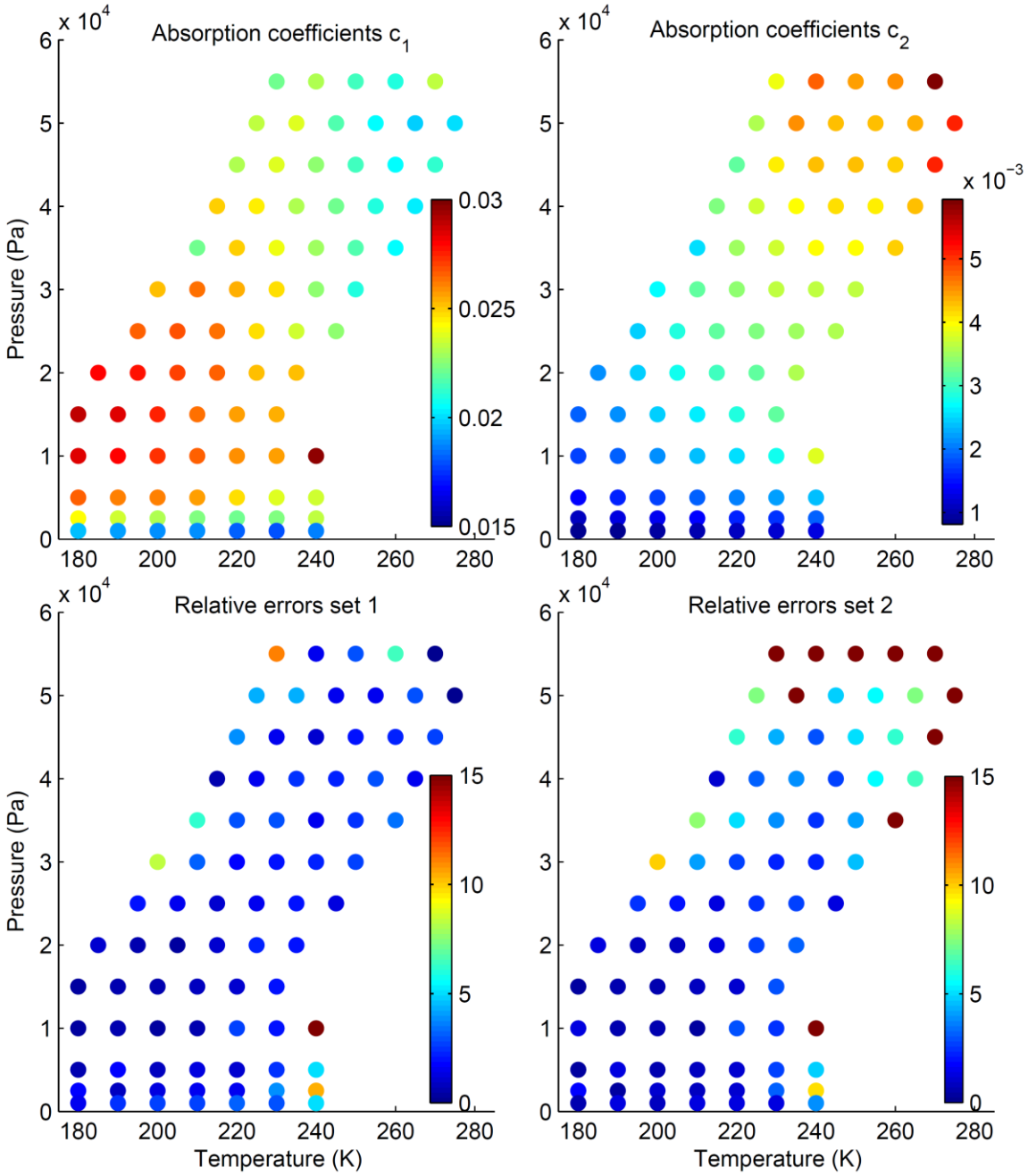

Fig. 6. Absorption coefficients for the two sets of IASI channels (top) and their corresponding average errors in percentage (bottom). Here the absorption coefficients and errors are shown for a SO_2 cloud of 10 DU (set 1) and 750 DU (set 2) respectively.

In the current implementation scheme, we use 5 different (P,T) pairs, corresponding to altitudes 7, 10, 13, 16, 25 km extracted from the IASI temperature, pressure profiles, to extract SO_2 at 5 different assumed altitudes. For each pixel, SO_2 columns are always calculated (however in the case of unphysical altitudes, i.e. an assumed height which is too low for the observed DBT, the result will be NaN).

Current limitations

The main limitations of the current algorithm are threefold. Firstly it is not suitable for SO_2 plumes/enhancements located in the lower troposphere (<5-7 km). This is especially true in the tropical band, as the sensitivity to the lower layers is determined by the total water vapour column. Secondly, it requires users to have an idea of the altitude of the plume. Especially for SO_2 in the range 5-10 km, the dependence of the column on the assumed altitude is large, and so errors made in the assumed altitude will translate into errors on the retrieved columns. This limitation is largely overcome by using SO_2 altitudes retrieved from the measurements themselves (see next section). The third and last limitation of the current algorithm is its moderate sensitivity to small column amounts. At present, there are several methods available building on the work of Walker et al. (2011) which make use of a larger spectral range with increased sensitivity.

3. THE IASI SO_2 ALTITUDE ALGORITHM

3.1 Algorithm description

The retrieval of the Brescia SO_2 altitude is described below. Note that most of the algorithm description below is reproduced verbatim from Clarisse et al. (2014).

Recently a very sensitive trace gas detection method was introduced for high spectral infrared measurements (Walker et al., 2011,2012). Consider a spectral retrieval of a trace gas total column $\hat{x}$ of the form (we assume that the background target columns x are negligible)

$$\hat{x} = (K^T\ S^{-1}\ K)^{-1} K^T S^{-1} (y - \bar{y})\ , \qquad (5)$$

with y the observed spectrum, $\bar{y}$ a background spectrum and K the derivative with respect to the target species. This is the maximum likelihood solution corresponding to the forward model $y = \bar{y} + Kx + \epsilon$ and with Gaussian instrumental noise ϵ characterised by a covariance matrix S (Rodgers, 2000). Here linearity is assumed as well as exact knowledge of all atmospheric parameters affecting the spectrum in the spectral range under consideration. In reality this knowledge is not available, and other unknown quantities (such as the surface temperature and water vapour for SO_2 retrievals) need to be taken into consideration. However, instead of retrieving these parameters, they can also be considered as permanent unknowns and incorporated in a generalised noise covariance matrix. In the linear case, such a solution is equivalent to the one obtained by simultaneously retrieving all interfering unknowns (von Clarmann et al., 2001; Rodgers, 2000). For species which are rarely observed in IASI spectra, constructing such a generalised noise covariance and associated background spectrum is easy, as it can be simply constructed from a random sample of spectra uncontaminated by the target species. This is the essence of the Walker et al. (2011, 2012) method. Despite its relative simplicity, test cases have revealed that it is about an order of magnitude more sensitive than previously used detection methods. The conditions of the retrieval, namely constant Jacobians K and linearity are usually not satisfied. The quantity $\hat{x}$ is therefore an apparent column which should be interpreted as a qualitative estimate of the column. For these reasons it is convenient to normalize this apparent column as

$$Z = \frac{K^T S^{-1} (y - \bar{y})}{\sqrt{K^T\ S^{-1}\ K}} \qquad (6)$$

This Z number is unitless and has a mean of zero and a standard deviation of one on uncontaminated spectra (Walker et al., 2011; Clarisse et al., 2013). It represents the number of standard deviations away from the average and the larger its value, the more likely it corresponds to an enhancement of the target species (Walker et al., 2012).

The real strength of the detection method stems from being able to use a large spectral range and a covariance matrix which characterises IASI measurements better than any traditional forward model could do. The SO_2 retrieval method presented in Carboni et al. (2012) uses a related approach to retrieve SO_2 columns and plume heights. It differs from the detection method in three ways. First, the covariance matrix is built from spectral residuals between observed spectra and spectra simulated by a forward model fed with the best possible knowledge of the local temperature and humidity profiles. Secondly, the maximum likelihood retrieval is replaced by an iterative Levenberg–Marquard retrieval with variable Jacobians. Here the SO_2 column is assumed to be confined to a narrow altitude band and the Jacobians are then calculated with respect to the column and the height of this band. The third difference is the use of a priori information and a covariance matrix which constrains the retrieval.

Retrievals performed in this way, then yield quantitative estimates of the column amounts and heights, as opposed to the apparent columns discussed above. The use of a generalised covariance matrix still preserves some of the advantages of the detection method, in particular enhanced sensitivity and being able to fully take into account the limitations of the forward model.

Here we propose a hybrid method to retrieve SO_2 plume heights. Let us define a Z function

$$Z(h) = \frac{K_h^T S^{-1}(y - \bar{y})}{\sqrt{K_h^T S^{-1} K_h}} \qquad (7)$$

with K_h the Jacobian with respect to the SO_2 partial column at an altitude h. When an observed spectrum contains a detectable amount of SO_2, this Z function should attain values significantly larger than 1. The Jacobians K_h contain the SO_2 signature that can be expected at an altitude h, and the Z function should therefore peak at h. Another way of seeing this is that Eq. (7) is a covariance weighted normalized projection (Clarisse et al., 2013) of the observed spectrum onto a SO_2 signature relevant to the different heights. When Z reaches its maximum there is maximal overlap between the observed spectrum and the SO_2 signature at that altitude. Simply calculating $Z(h)$ for different altitudes h, and finding the maximum thus gives a viable and fast way of estimating SO_2 plume altitude. Example Jacobians in the range 1300–1410 cm−1 and $Z(h)$ for different observed spectra are presented in Fig.7. For this example, large differences in the Jacobians can be observed up to an altitude of 15 km. This is logical as most of the altitude information comes from interference of the SO_2 absorption lines with the water vapour band. This is reflected in the $Z(h)$ profiles shown on the right. At low altitudes, these peak sharply, and become broader as the altitude increases.

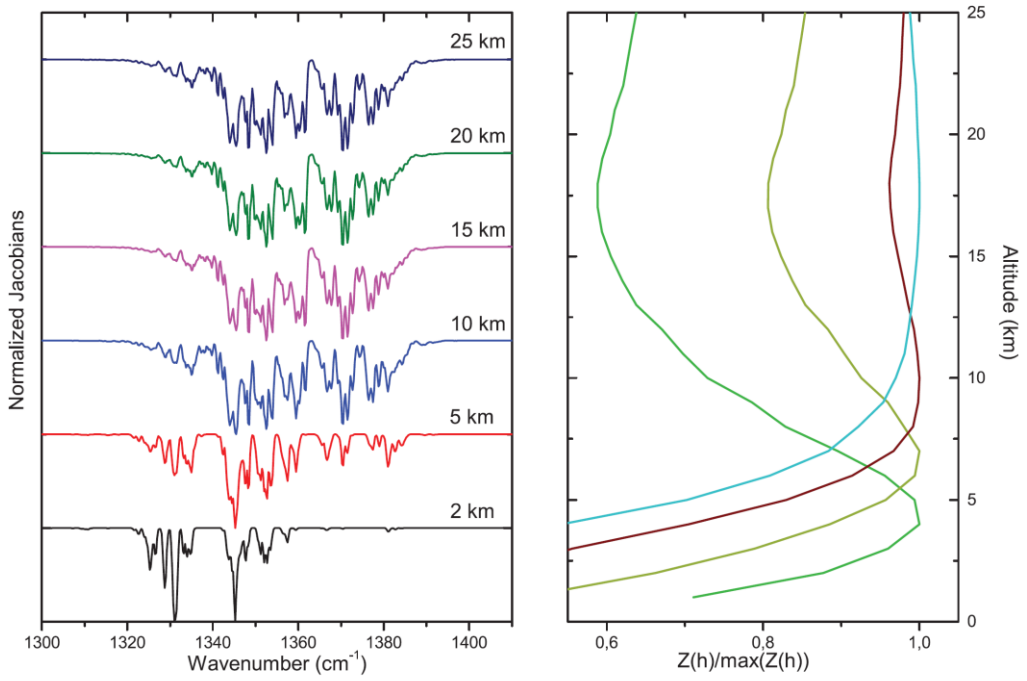

Fig. 7. (Left) Jacobians with respect to a SO_2 layer at different altitudes. They have been normalised and offset for display purposes. (Right) The Z function acting on different observed IASI spectra of Nabro. The values have been normalised to ease comparison.

To test the theoretical accuracy of this method for different altitudes, 10 000 forward simulations of 5 DU SO_2 clouds between 1 and 30 km were carried out. To make the simulation as realistic as possible, spectral noise was added to these spectra. This noise was generated from the multivariate normal distribution with the mean bias and covariance matrix used for the quantitative SO_2 column retrievals (see end of this section). Calculating spectra in this way is a realistic way of simulating real observed spectra because biases in the forward model are removed, and because instrumental noise is added. However, note that the atmospheric parameters used in the simulation are the same as the ones which were used to construct the Jacobians. Using this method we hence obtain upper bounds on the accuracy of the algorithm.

The results are summarised in Fig.8. As expected from the $Z(h)$ profiles shown in Fig.7, the best accuracy is achieved between 5 and 15 km with error bars below 500 m. Below 3 km the tropical atmosphere is almost opaque in the spectral range of interest due to water vapour, and the algorithm therefore loses its accuracy drastically (a dryer atmosphere would allow to penetrate lower down). Above 18 km, the error bar is almost constant at around 1.5 km. At these altitudes, the water vapour content in the atmosphere is low, and the fact that such a good sensitivity is achieved is related to pressure and temperature dependence of the SO_2 lines (Clerbaux et al., 2008). Although hard to see with the naked eye on apodized IASI spectrum, the simulation demonstrates that altitude information is contained in the spectrum even in the stratosphere.

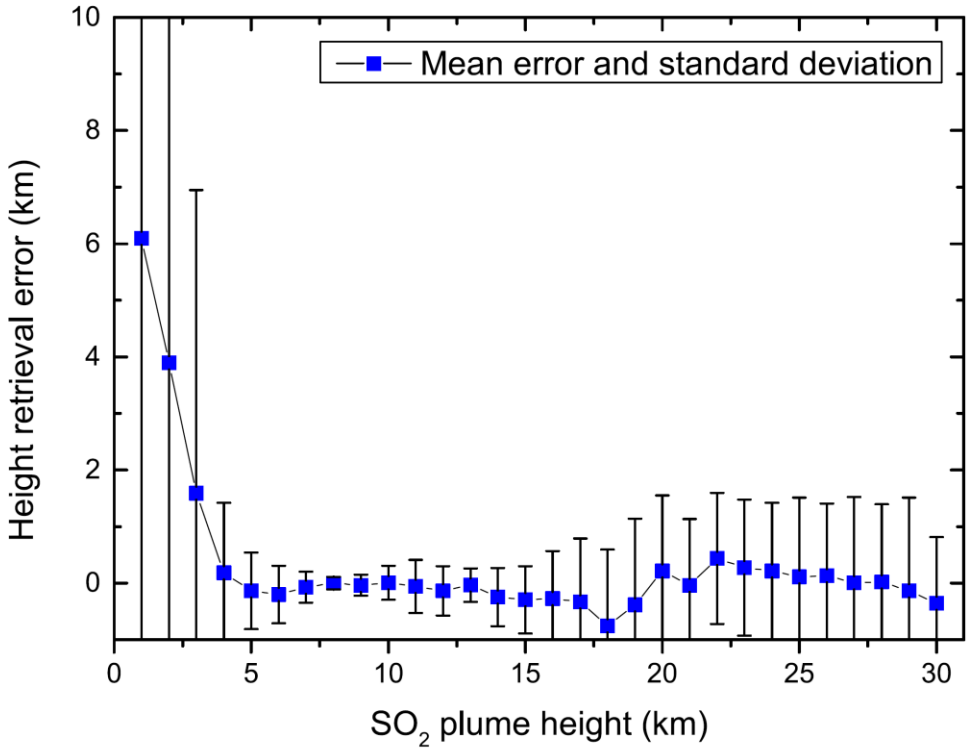

Fig. 8. Theoretical height retrieval error biases and standard deviations constructed from a simulation of 10 000 IASI spectra with SO_2 altitudes between 1 and 30 km.

Another appealing aspect of the algorithm is the performance on scenes with overlaying meteorological clouds. Cloudy scenes are at no stage in the algorithm treated separately. Hence, it could be argued that as water in the gas and in the liquid phase have a similar broad band extinction across the infrared spectral region that these will have an important effect. However, as we will show later, clouds seem to have little effect on the retrieved altitudes of this hybrid method, as long as they are not completely masking the SO_2 layer below. The reason is that while the broad extinction of clouds and water vapour is present in the Jacobians, these also exhibit the sharp spectral lines of water vapour in the gas phase, which are not found in clouds.

This hybrid method has the benefit of relying on the for-ward model just for its Jacobians. These can be precalculated once and the remaining calculations then become trivial. In other words, this method is suitable for near real time applications and can be implemented in operational centres with minimal computational resources. It would for instance be a good candidate for implementation in the SACS project (Brenot et al., 2013), dedicated to timely warning of volcanic plumes. Another benefit is that the algorithm uses no a-priori information or constraints on its retrieval. Especially for smaller loadings, there is always the possibility of a constrained height retrieval algorithm to get stuck in a local minimum near its a priori. It also has some disadvantages, the main one is probably its performance for heavily saturated plumes. In this case, the Jacobians that are calculated in the neighbourhood of small loadings are no longer representative. Fortunately, saturation occurs only in very young plumes, and even in these cases, altitudes can be estimated from the plume edges, away from saturation.

In what follows, we have interpolated pixels with a Z value larger than 250 or an altitude larger than 23 km from nearby pixels. The latter condition was found to be good at removing isolated rogue detections just above or below IASI's detection limit. Jacobians were calculated with Atmosphit (Coheur et al., 2005) using average atmospheric conditions representative for 10°×20° latitude/longitude boxes in the Northern Hemisphere in June 2011. Average water vapour and temperature profiles were calculated in each box from the Eumetsat IASI L2 data of several days in June 2011. In each case, Jacobians were generated representative for plumes between 1 and 30 km in steps of 1 km, with a 1 km thick layer of 5 DU of SO_2. For each specific observation, local Jacobians were then obtained using a bilinear interpolation of the four closest grid boxes. For operational applications Jacobians would need to be precalculated for such boxes and different time-periods of the year. For the construction of the global mean spectrum $\bar{y}$ and the global error covariance matrix S we used one million random IASI spectra selected from all periods of the year from around the globe. Spectra with observable SO_2 features were filtered out recursively (analogously as was done in Clarisse et al., 2013).

4. REFERENCES

Brenot, H., Theys, N., Clarisse, L., van Geffen, J., van Gent, J., Van Roozendael, M., van der A, R., Hurtmans, D., Coheur, P.-F., Clerbaux, C., Valks, P., Hedelt, P., Prata, F., Rasson, O., Sievers, K., and Zehner, C.: Support to Aviation Control Service (SACS): an online service for near real-time satellite monitoring of volcanic plumes, Nat. Hazards Earth Syst. Sci. Discuss., 1, 5935–6000, doi:10.5194/nhessd-1-5935-2013, 2013.

Camy-Peyret, C. and Eyre, J. The IASI Science Plan. Technical report, A Report From The IASI Sounding Science Working Group, 1998.

Carboni, E., Grainger, R., Walker, J., Dudhia, A., and Siddans, R.: A new scheme for sulphur dioxide retrieval from IASI measurements: application to the Eyjafjallajökull eruption of April and May 2010, Atmos. Chem. Phys., 12, 11417–11434, doi:10.5194/acp-12-11417-2012, 2012.

Chevallier, F.: Sampled databases of 60-level atmospheric profiles from the ECMWF analyses, Tech. rep., Eumetsat/ECMWF SAF Programme, Research Report No. 4, 2001.

Clarisse, L., Hurtmans, D., Prata, A. J., Karagulian, F., Clerbaux, C., Mazière, M. D., and Coheur, P.-F.: Retrieving radius, concentration, optical depth, and mass of different types of aerosols from high-resolution infrared nadir spectra, Appl. Optics, 49, 3713–3722, doi:10.1364/AO.49.003713, 2010a.

Clarisse, L., Prata, F., Lacour, J.-L., Hurtmans, D., Clerbaux, C., and Coheur, P.-F.: A correlation method for volcanic ash detection using hyperspectral infrared measurements, Geophys. Res. Lett., 37, L19806, doi:10.1029/2010GL044828, 2010b.

Clarisse, L., Hurtmans, D., Clerbaux, C., Hadji-Lazaro, J., Ngadi, Y. and Coheur, P. F.: Retrieval of sulphur dioxide from the infrared atmospheric sounding interferometer (IASI), *Atmos. Meas. Tech., 5*, 581-594, doi:10.5194/amt-5-581-2012, 2012.

Clarisse, L.; P.-F. Coheur; F. Prata; J. Hadji-Lazaro; D. Hurtmans and C. Clerbaux. A unified approach to infrared aerosol remote sensing and type specification. Atmos. Chem. Phys., 13: 2195-2221, 2013.

Clarisse, L.; P.-F. Coheur; N. Theys; D. Hurtmans and C. Clerbaux. The 2011 Nabro eruption, a SO2 plume height analysis using IASI measurements. *Atmos. Chem. Phys*., 14: 3095-3111, 2014.

Clerbaux, C., Coheur, P.-F., Clarisse, L., Hadji-Lazaro, J., Hurtmans, D., Turquety, S., Bowman, K., Worden, H., and Carn, S.: Measurements of SO2 profiles in volcanic plumes from the NASA Tropospheric Emission Spectrometer (TES), Geophys. Res. Lett., 35, L22807, doi:10.1029/2008GL035566, 2008.

Clerbaux, C., Boynard, A., Clarisse, L., George, M., Hadji-Lazaro, J., Herbin, H., Hurtmans, D., Pommier, M., Razavi, A., Turquety, S., Wespes, C. and Coheur, P. F. Monitoring of atmospheric composition using the thermal infrared IASI/MetOp sounder. *Atmos. Chem. Phys*., 9(16):6041-6054, 2009.

Coheur, P.-F., B. Barret, S. Turquety, D. Hurtmans, J. Hadji-Lazaro, and C. Clerbaux (2005), Retrieval and characterization of ozone vertical profiles from a thermal infrared nadir sounder. J. Geophys. Res., 110, D24303, doi:10.1029/2005JD005845.

Flaud, J.-M., Lafferty, W., and Sams, R.: Line intensities for the ν_1, ν_3, and $\nu_1+\nu_3$ bands of $^{34}SO_2$, *J. Quant. Spectrosc. Radiat. Transfer*, 110, 669–674, 2009.

Hilton, F., August, T., Barnet, C., Bouchard, A., Camy-Peyret, C., Clarisse, L., Clerbaux, C., Coheur, P.-F., Collard, A., Crevoisier, C., Dufour, G., Edwards, D., Faijan, F., Fourrié, N., Gambacorta, A., Gauguin, S., Guidard, V., Hurtmans, D., Illingworth, S., Jacquinet-Husson, N., Kerzenmacher, T., Klaes, D., Lavanant, L., Masiello, G., Matricardi, M., McNally, T., Newman, S., Pavelin, E., Péquignot, E., Phulpin, T., Remedios, J., Schlüssel, P., Serio, C.,

Strow, L., Taylor, J., Tobin, D., Uspensky, A. and Zhou, D. Hyperspectral Earth Observation with IASI. *Bull. Am. Meteorol. Soc., 93(3)*, 347-370, doi: 10.1175/BAMS-D-11-00027.1, 2012.

Karagulian, F., Clarisse, L., Clerbaux, C., Prata, A. J., Hurtmans, D., and Coheur, P. F.: Detection of volcanic SO_2, ash and H_2SO_4 using the IASI sounder, *J. Geophys. Res.*, 115, D00L02, doi:10.1029/2009JD012786, 2010.

NASA (1976) U.S. Standard Atmosphere, U.S. Government Printing Office, Washington, D.C.

Prata, A., Gangale, G., Clarisse, L., and Karagulian, F.: Ash and sulfur dioxide in the 2008 eruptions of Okmok and Kasatochi: Insights from high spectral resolution satellite measurements, *J. Geophys. Res.*, 115, D00L18, doi:10.1029/2009JD013556, 2010.

Rodgers, C.: Inverse methods for atmospheric sounding: theory and practice, series on atmospheric, oceanic and planetary physics, World Scientific, 2000.

Rothman, L., Gordon, I., Barbe, A., Benner, D., Bernath, P., Birk, M., Boudon, V., Brown, L., Campargue, A., Champion, J.-P., Chance, K., Coudert, L., Dana, V., Devi, V., Fally, S., Flaud, J.-M., Gamache, R., Goldman, A., Jacquemart, D., Kleiner, I., Lacome, N., Lafferty, W., Mandin, J.-Y., Massie, S., Mikhailenko, S., Miller, C., Moazzen-Ahmadi, N., Naumenko, O., Nikitin, A., Orphal, J., Perevalov, V., Perrin, A., Predoi-Cross, A., Rinsland, C., Rotger, M., ˇSimeˇcková, M., Smith, M., Sung, K., Tashkun, S., Tennyson, J., Toth, R., Vandaele, A., and Auwera, J. V.: The HITRAN 2008 molecular spectroscopic database, *J. Quant. Spectrosc. Radiat. Transfer*, 110, 533–572, doi:10.1016/j.jqsrt.2009.02.013, 2009.

von Clarmann, T., Grabowski, U., and Kiefer, M.: On the role of non-random errors in inverse problems in radiative transfer and other applications, J. Quant. Spectrosc. Ra., 71, 39–46, doi:10.1016/S0022-4073(01)00010-3, 2001.

Walker, J. C.; Dudhia, A. and Carboni, E.; An effective method for the detection of trace species demonstrated using the MetOp Infrared Atmospheric Sounding Interferometer. Atmos. Meas. Tech., 4, 1567-1580, 2011.

Walker, J. C., Carboni, E., Dudhia, A., and Grainger, R. G.: Improved detection of sulphur dioxide in volcanic plumes using satellite-based hyperspectral infrared measurements: Application to the Eyjafjallajökull 2010 eruption, J. Geophys. Res, 117, D00U16, doi:10.1029/2011JD016810, 2012.

Watson, I., Realmuto, V., Rose, W., Prata, A., Bluth, G., Gu, Y., Bader, C., and Yu, T.: Thermal infrared remote sensing of volcanic emissions using the moderate resolution imaging spectroradiometer, *J. Volcanol. Geoth. Res.*, 135, 75–89, 2004.

5. ANNEX: EXPLANATION OF SYMBOLS USED IN THE ATBD

Brightness Temperature	Radiance	Comments
T_s	$L_s(\nu)$	Radiance (and corresponding brightness temperature) measured at the sensor
T_{ucb}	$L_{ucb}(\nu)$	upwelling radiance (and corresponding brightness temperature) at the cloud base
T_c	$L_c(\nu)$	Temperature of the cloud (and corresponding radiance)
T_c^*	$L_c^*(\nu)$	virtual cloud temperature $T_c^* = T_c - [H_2O]/10^{21}$, with [H2O] the partial column of water (in molecules cm^{-2}) above the SO_2 layer
K_h		Jacobian with respect to the SO_2 partial column at an altitude h.